Applied Energy 242 (2019) 782–796

Contents lists available at ScienceDirect

Applied Energy

journal homepage: www.elsevier.com/locate/apenergy

Performance of firebrick resistance-heated energy storage for industrial heat applications and round-trip electricity storage

Daniel C. Stack*, Daniel Curtis, Charles Forsberg

Massachusetts Institute of Technology, 77 Massachusetts Avenue, Cambridge, MA 02139, United States

HIGHLIGHTS

- FIRES thermal energy storage is proposed as an affordable path to decarbonization.
- Charge, discharge and heat leakage simulations are presented over the design space.
- FIRES costs are estimated and discussed with respect to performance tradeoffs.
- Flexible cycling and storage duration can accommodate intermittent electricity.
- Electricity market case study shows short payback period and reduced emissions.

ARTICLE INFO

Keywords:
Energy storage
Renewable energy
Nuclear energy
Decarbonization
Energy economics

ABSTRACT

In the absence of an affordable and deployable energy storage option, the intermittency of renewable energy creates mismatches in supply and demand that limit the viability of a low-carbon electricity grid. High temperature electrically-heated thermal energy storage (E-TES) is a largely unexplored approach to alleviating the problem of low-value renewable energy. Evaluated herein is one E-TES concept, called Firebrick Resistance-Heated Energy Storage (FIRES), that stores electricity as sensible high-temperature heat (1000–1700 °C) in ceramic firebrick, and discharges it as a hot airstream to either (1) heat industrial plants in place of fossil fuels, or (2) regenerate electricity in a power plant. FIRES storage media and heater options are reviewed, and discharge cycling is simulated with Crank-Nicolson finite difference schemes and evaluated over the parameter design space. We report that systems of 100–1000 s MWh may be cycled daily, and discharged at a constant heat rate typically for 70–90% of the storage capacity. Traditional insulation can reasonably limit heat leakage to less than 3% per day. Preliminary cost estimates indicate a system cost near $10/kWh, substantially less expensive than batteries. Northwestern Iowa market analysis shows payback within 2 years and economic profitability.

1. Introduction

The large-scale introduction of renewable energy into the electricity grid can cause large reductions in wholesale electricity prices, including negative prices, at times of high solar or wind output [1–3]. The collapse of electricity prices hurts the economics of high-capital-cost low-operating-cost generators, including solar, wind and nuclear plants, and limits the feasibility of a low-carbon energy grid. However, grid-scale electricity storage remains expensive and difficult to deploy. Pumped hydro and compressed air storage (CAES), although proven and affordable, are limited in their deployment by geographical requirements [4]. Current prices for batteries, the most deployable option, typically range between $250 and $500/kWh [5], with long-term prices projected to remain $150/kWh or more [6,7]. As a result, wasteful curtailment of wind and solar generation is presently the common solution to excess power production [1,3]. Curtailment and revenue collapse will increase with further renewable expansion in the absence of affordable storage.

There is an option to instead sell low-value and otherwise curtailed renewable generation to the industrial heating market, or to high-temperature power plants, by means of electrically-heated thermal energy storage. Thermal energy storage (TES) has long been employed in a variety of applications, such as heat recovery from combustion flue gases [8,9], and more recently in concentrated solar power (CSP) plants to store solar energy for nighttime electricity generation [10,11]. Where these TES systems capture heat from combustion or the sun, electrically-heated TES (E-TES) systems capture excess electricity as heat. E-TES has had little or no exploration at industrial scale, but has

* Corresponding author.
E-mail addresses: dcstack@mit.edu (D.C. Stack), djcurtis@mit.edu (D. Curtis), cforsber@mit.edu (C. Forsberg).

https://doi.org/10.1016/j.apenergy.2019.03.100
Received 8 October 2018; Received in revised form 15 February 2019; Accepted 9 March 2019
Available online 20 March 2019

been proven on the residential and commercial scales in the form of firebrick air channels with integrated electrical resistance heaters, which store off-peak electricity as heat for on-demand room heating (700–800 °C storage temperature, 10–100 s kWh capacity). In China, scaled up firebrick units have been deployed at 10 MWh for large commercial complexes and district heating projects, as part of their "Coal to electricity" anti-pollution policies [12]. Existing firebrick storage units cost as little as $15/kWh, an order of magnitude lower than the lowest price scenario for batteries.

A scaled-up form of firebrick E-TES, referred to hereon as "firebrick resistance-heated energy storage" (FIRES) [13,14], is a promising option for capturing and transferring surplus low-price electricity to the industrial heating market, or for installation in power plants for regeneration of electricity. The temperatures and heat rates necessary for coupling with industrial furnaces and power plants (1000–1700 °C, 10–100 s MW) are already seen in non-electric firebrick TES systems, such as the regenerative heat exchangers of blast furnaces [9].

FIRES coupled with industrial furnaces or refineries may be installed upstream of the fossil fuel combustion step and heat the air for partial or complete replacement of fossil fuels. From a market perspective, the much larger size of industrial heating demands compared to electricity generation (21 quads versus 12.6 quads nationally [15]) allows the industrial heating sector to easily absorb low-value electricity. Rather than experiencing near-zero or negative prices, electrifying enough industrial furnaces and refineries with FIRES would allow electricity to be valued regionally at its equivalent fossil fuel heating cost, preventing price collapse. Selling surplus electricity to the heating market via FIRES would ensure revenue to low-carbon generators, while also reducing fossil fuel consumption.

FIRES may also be coupled to traditional power plants for electricity regeneration, acting as an electricity storage device for low-carbon generators. Fossil fuel plants may shut down and store excess electricity in FIRES during peak solar or wind production, and later discharge the heat in place of fossil fuels to run the power cycle. For a well-insulated system, the round-trip efficiency of FIRES is effectively equal to the power cycle efficiency of the coupled plant: near 60% for modern natural gas combined cycle (NGCC) power plants. The coupling of FIRES with power plants for round-trip electricity production offers an alternative storage option to batteries that takes advantage of existing turbomachinery and is not dependent on geography.

In the long term, FIRES heat storage may be coupled to generation-IV nuclear air-Brayton combined cycles (NACC) or similar CSP cycles. One NACC design is in development by UC Berkeley [16], which allows for heat addition by alternative sources such as natural gas, hydrogen or stored heat. By adding FIRES heat to the NACC and boosting turbine inlet temperatures above that produced by the nuclear reactor, the resulting round-trip efficiency is reported as 66.4%. Turbine advances and heat addition above the reported boosted temperature of 1065 °C may increase this efficiency near 70%. FIRES also offers the coupled nuclear plant the option of storing its own electricity rather than selling at a loss or ramping down the reactor during times of low demand.

Steps toward using E-TES for generating electricity have been taken by industry. One E-TES concept under development is that of electrically-heated crushed rock storage by Siemens Gamesa [17] for coupling with steam turbines. The technology holds promise for providing affordable storage, and a 30 MWh pilot plant is nearing its 2019 completion date. However the rock is reportedly heated to 600 °C, which limits its application to low efficiency power cycles. The high temperature firebrick and higher performance heating options of FIRES is one potential pathway to coupling E-TES with high temperature industry and more efficient power cycles. Gas turbines coupled with firebrick is already being developed for adiabatic compressed air energy storage (A-CAES). Zunft et al. have been developing a grid-scale A-CAES technology through the ADELE and ADELE-ING projects [18], which makes use of a large firebrick regenerator (300 MW_t, 1200 MWh_t) contained within a prestressed concrete pressure vessel to store the compression heat of air. The system uses low-value electricity to compress air to approximately 70 bar for storage in an underground salt cavern, but first runs the hot air through the firebrick regenerator to cool it from approximately 560 °C to 40 °C. The air is reheated through the regenerator before discharging to the turbine for a round-trip efficiency near 70% [19,9]. The key difference between ADELE and FIRES is that the latter operates at lower cycle pressures (20 bar or less) and higher temperatures (1000–1700 °C), and has integrated heaters to charge it. Additionally, FIRES is designed to be implemented with existing power plants, such that it does not require special geography or additional turbomachinery to achieve round-trip electricity storage.

Beyond the work in these areas, several studies of the design options of grid-scale TES systems have been undertaken. Gil et al. [11] reviews a wide option space of TES designs and modelling methods, including different sensible and latent heat material candidates and solid, liquid and packed bed inventory configurations. However, the designs are generally discussed and analyzed with respect to their heat recovery of flue gases or for CSP storage; none of the designs or materials are discussed with respect to their E-TES potential, i.e. integration with an electrical input. In this context temperatures rarely exceeding 500–800 °C, and pressures are near-atmospheric.

With respect to previous studies, FIRES has two defining features that demand exploration: (1) FIRES is charged electrically. Identifying the options and challenges for electrically heating a large thermal mass is key in evaluating the viability of the FIRES concept. Charging via electricity also enables much higher storage temperatures than those seen in other TES systems, which impacts materials selection and system design compared to previous studies; (2) the application space of FIRES is large, and spans a continuum of operating temperatures, pressures and heat rates across the industrial heating sector and various power plant technologies, whereas most previous studies are concerned with finding the optimal design for predefined parameters. As such, the performance characteristics of FIRES over a continuum of operating conditions is valuable.

This paper introduces and evaluates the performance of a FIRES system designed to couple with high-heat industrial plants and power cycles. The FIRES system is described, and candidate storage media and electrical heating options are reviewed. The discharge modeling is discussed, and results are presented for various materials, dimensions, system capacities, operating temperatures and pressures, and discharge rates. Results are analyzed with respect to different performance metrics, including thermal shock considerations. Charge results for metallic heater wires and heat leakage calculations are presented briefly. Afterward cost estimates of major system components for a "base case" FIRES unit are summarized, and market performance is evaluated in a Western Iowa (high wind penetration) energy market.

2. System description

FIRES consists of a firebrick storage medium of relatively high heat capacity and density. The firebrick is laid in a pattern that forms a brickwork of air channels. FIRES is "charged" using resistance heaters integrated within the air channel brickwork. FIRES is "discharged" by blowing cold air through the hot brickwork. The heated airstream can be coupled to most combustion-driven industrial processes. The brickwork is surrounded by insulative firebrick and a steel vessel that minimize heat leakage and maintain safe temperatures for surrounding structures. The brickwork, insulation and containment are similar to high-temperature firebrick regenerators that are commonplace in industrial glassmaking and steelmaking [8,9]. Fig. 1 below shows the regenerative Cowper stoves used in blast furnaces and several common geometries of the bricks that make up the brickworks of regenerators.

A chimney-style firebrick regenerator system was chosen due to several application-specific advantages over other TES configurations such as molten salt, phase change materials (PCM), or packed bed solid storage. A key goal of the FIRES design is to deliver heat to airstreams,

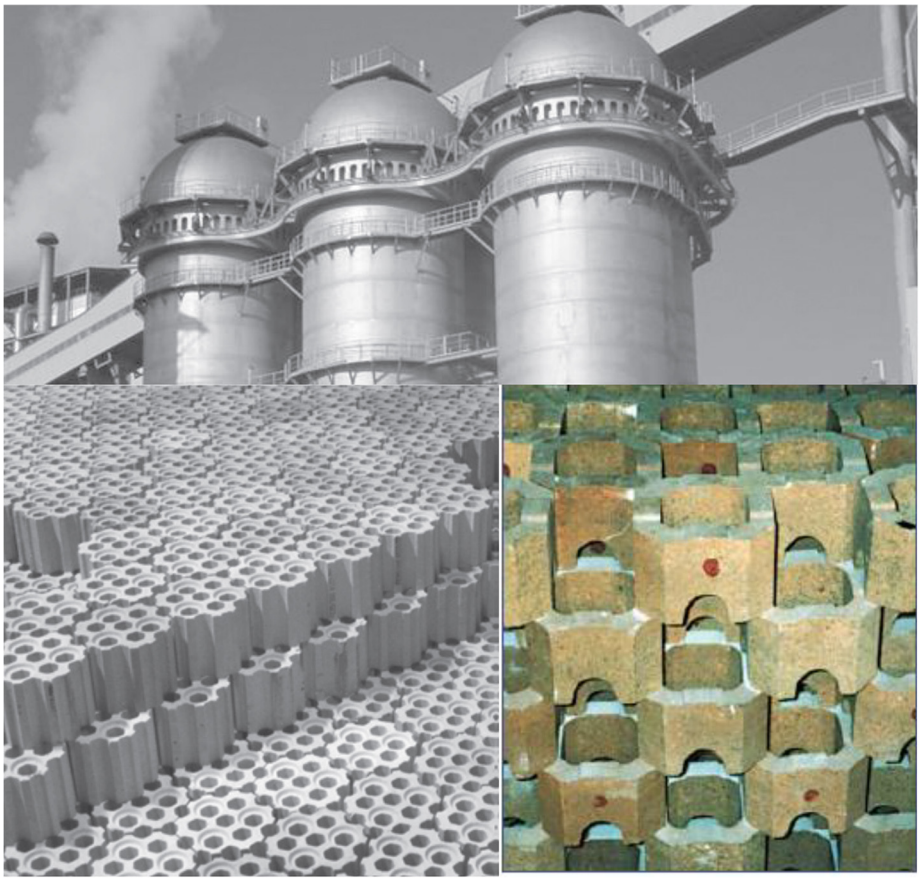

Fig. 1. Regenerative firebrick Cowper stoves (top) and common brickwork options (bottom).

in place of fossil fuel heat, at temperatures exceeding 1000 °C. Reviews of PCM and liquid options do not generally identify options or experiences above 800 °C [10]. Moreover, achieving leakage-free boundaries and effective heat transfer between the electrical heating components, liquid storage media and airstream presents a unique set of design challenges. These challenges are dramatically increased in the presence of high pressures such as in power cycle applications. By comparison, solid storage designs such as a packed bed or chimney brickwork regenerator transfer heat directly to air and can be included within the pressure boundary of an application. Of these two options, the bricks of a chimney brickwork allow for easier integration and replacement of heating elements, and are customizable to form favorable geometries. In addition to possessing the key requirements of heat storage media [10,11], such as excellent chemical and mechanical stability, a large specific heat capacity, and affordability at scale, firebrick materials have excellent operating temperatures capable of handling the peak performance of conventional electrical heating options. Firebrick regenerators such as Cowper stoves are a mature technology with proven performance at the temperatures and heat rates needed for FIRES: peak temperatures of 1600 °C, heat rates up to 300 MW [9], and lifespans of 20–30 years [20], with hourly cycling and nearly continuous operation [21]. In these conditions individual firebricks have been demonstrated to survive many thousands of cycles. A chimney-style FIRES unit was therefore chosen for analysis herein. However other FIRES and E-TES concepts are possible.

Fig. 2 shows a schematic of FIRES coupled with a generic plant. FIRES is installed upstream of the traditional fossil fuel heat source of the plant, and is charged during times of cheap electricity. Charging may occur simultaneously with discharge. When heat is demanded, the airstream of the heating process first passes through FIRES to be heated; if the temperature of air exiting the brickwork is hotter than desired by

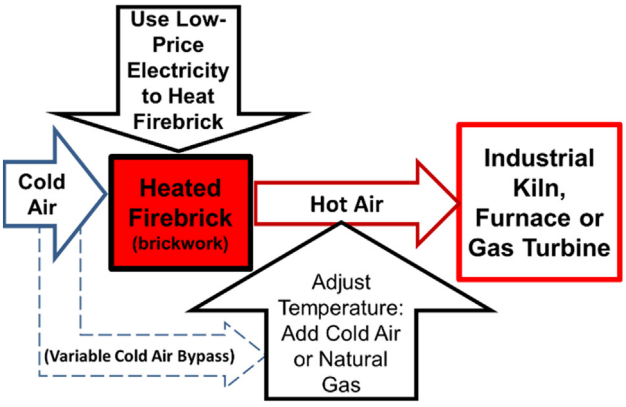

Fig. 2. Schematic of FIRES coupled with industrial heating application.

the application, a portion of the air is diverted to bypass the brickwork, and is recombined at the brickwork outlet to appropriately adjust the temperature. As the brickwork is cooled, the bypassed flow is gradually reduced and redirected through the brickwork such that the application operating temperature is always matched. When the brickwork output temperature drops below that desired by the application, the remaining heat demand is delivered by the traditional fossil fuel burner downstream of the firebrick, with FIRES serving as a preheater. Pressure losses through the brickwork may be overcome by using the existing blower system of the industrial site or by augmenting with additional fans to push air into FIRES. The flow of air is controlled by dampers at the brickwork and bypass inlets. In gas turbines, FIRES is implemented between the compression step and the combustion step of the power cycle, and experiences the pressure and temperature at the compressor

Table 1
Properties of candidate firebrick and heaters.

Candidate firebrick properties										
Name	Chemical	T_{melt} [23]	Thermal conductivity [24,25] (@ 25 °C, 500 °C, 1200 °C)			Density [23]	Specific heat [23] (@ 25 °C)	Estimated energy density (ΔT = 1000 °C)	Estimated material cost (sale price)	Estimated energy cost
–	–	°C	W/mK			kg/m^3	kJ/kgK	MWh/m^3	$/ton	$/kWh
Alumina	Al_2O_3	2054	37	10	5.7	3987	0.84	0.93	500	2.14
Magnesia	MgO	2852	52	13	7.7	3581	0.96	0.96	500	1.87
Silicon carbide	SiC	2093	114	55	31	3160	0.75	0.66	1500	7.18

Candidate heater properties			
Heater type	Peak operating temperature	Max recommended surface load	
		@ Typical temp	@ High temp
–	°C	kW/m^2	kW/m^2
Nickel-chrome (Ni-Cr) [26]	1250	35–100 (800 °C)	10–25 (1100 °C)
Iron-chrome-aluminum (Fe-Cr-Al) [26]	1425	50–120 (800 °C)	20–35 (1300 °C)
Silicon carbide (SiC) [27]	1650	100–150 (1200 °C)	25–30 (1600 °C)
Molybdenum disilicide ($MoSi_2$) [28]	1850	200–220 (1500 °C)	80–120 (1750 °C)

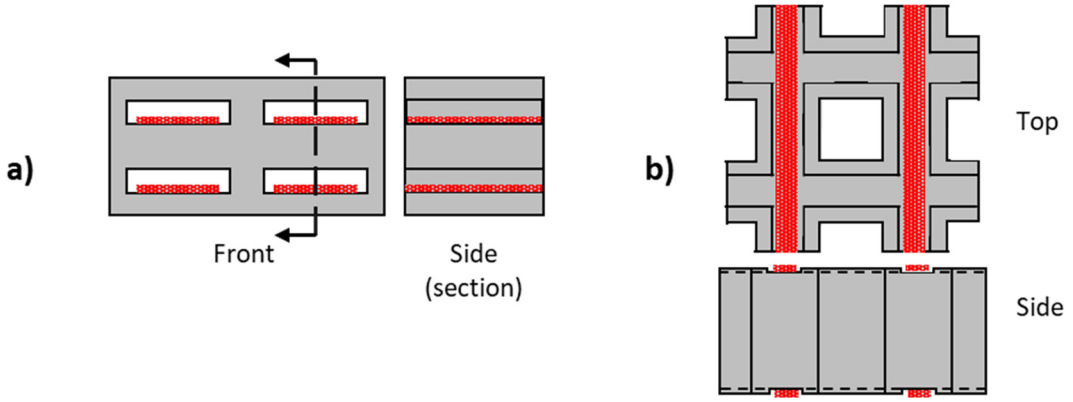

Fig. 3. Different brick-heater configurations that avoid heater supports. (a) For a horizontal FIRES unit, narrow horizontal air channels support metallic heaters and maximize surface area between element and walls. (b) For a vertical FIRES unit, thin cross-channels are formed perpendicular to the air channels.

exit. Air is transported to FIRES via an exit guide vane and diffuser into an aerodynamic scroll case similar to those designed for intercooling [22].

Properties of firebrick materials and heater candidates are shown in Table 1. The firebrick material influences system size and heat transfer, which relates to charge and discharge rates. Alumina and magnesia are similar in terms of cost, storage capacity and thermal conductivity. Alumina is commonly the ceramic of choice in the chimney-style bricks shown in Fig. 1. Silicon carbide is more expensive and less energy dense but is more thermally conductive, which is appealing in applications that demand fast heat discharge rates and exceptional thermal shock resistance. Silica is another common and inexpensive component in firebricks but possesses relatively poor thermal conductivity and lower energy density than the others listed; its use may be cost-effective but with a tradeoff in performance. It is worth noting that a survey of prices from online vendors indicated typical alumina and magnesia prices of a few hundred dollars per ton (assumed $500/ton for estimates herein), as compared to the $2000/ton cited for magnesia bricks by [11]. Actual costs will vary depending on location, availability of raw materials, and shipping costs.

Different heater types have different peak temperatures, surface loading and installation constraints. The peak temperature of FIRES must be chosen while considering the operating temperature of the industrial process, which may be anywhere from approximately 100–1600 °C [10,29]. Peak temperature also determines energy density, by setting the temperature gain during charge. For a 1000 °C temperature gain, heat storage capacity of low-porosity firebrick ranges from 0.5 to 1 MWh/m^3. It is generally best to operate heaters 100–200 °C lower than their peak temperature to avoid short heater lifetimes [30]; for example, metallic heaters experience roughly a doubling of lifetime by every 50 °C reduction of operating temperature [26], primarily due to oxidation kinetics. Material thickness also has a direct relationship to element life, by allowing for the formation of new protective oxide, at the tradeoff of higher element cost per surface area.

Metallic alloy heaters such as nickel-chrome (Ni-Cr) and iron-chrome-aluminum (Fe-Cr-Al) [26] have lower peak temperatures (up to 1425 °C) and lower surface loading compared to ceramic heaters, but are generally the most cost-effective and versatile in installation. They are sold in customizable lengths of straight or corrugated wires and strips that can be combined in series or parallel to achieve a desired circuit resistance for the given power supply setup. The wires or strips can span long distances, such as the length or width of the brickwork, but must be supported against gravity. This is commonly done in furnace applications using refractory hooks, staples, or grooves. One way to avoid the need for hooks and grooves in the brickwork is to lay the wires horizontally along the brickwork itself, by either orienting the air channels horizontally or designing bricks to form small cross-channels when stacked. Fig. 3 shows brick designs for each option. Heaters may be replaced by pulling them out along the plenum at either end of the channels or by opening parts of the containment for maintenance.

Silicon carbide (SiC) heaters [27] and molybdenum disilicide ($MoSi_2$) heaters [28] reach significantly higher temperatures than

metallic heaters and have higher surface loading but are generally more expensive. They are also of limited length, typically 2.5 m maximum, and must be cantilevered against the wall or ceiling across the thermal boundary of the containment. This limits the ability of SiC and $MoSi_2$ elements to deliver heat to the center of a large brickwork. One approach to effectively use SiC or $MoSi_2$ heaters in FIRES is to build several smaller-diameter containments rather than one large one so that cantilevered heaters can reach the center of the brickwork. Another option is to primarily install heaters upstream in the plenum region of the containment and deliver heat by convection. Each option has practical tradeoffs regarding performance, the merits of which are application-specific.

In the near term, metallic heaters are expected to be the preferred heating method for FIRES, though higher temperature applications may make use of the higher temperatures and longer life of SiC or $MoSi_2$ heaters. With more development, another possibility not discussed herein is to use electrically conductive firebrick, which may act as both the heating element and the storage medium. Direct resistance heating (DRH) or induction heating of firebrick are areas of ongoing work [31].

Insulation is designed with respect to how long heat is expected to be stored. Daily cycles will warrant less insulation than weekly cycles. Containment is designed with respect to the operating pressure of the application; most industrial heating systems operate near atmospheric pressure, whereas FIRES coupled with gas turbines will operate at high pressures. The latter will therefore require a pressure vessel of either steel or prestressed concrete.

3. Discharge

3.1. Modeling and simulation

The heat transfer of a FIRES discharge period was simulated numerically considering a characteristic “cell” of a square chimney brickwork, made up of a single air channel and surrounding firebrick. By virtue of the repeated cell geometry of the brickwork, and with the assumption of uniform pressure drops and temperatures, one cell can be used to describe the entire FIRES system. Although uniform conditions for all cells is not achievable in practice, proper design of the heater integration, insulation, and air plenums should create relatively uniform conditions. For simplification to 1-dimensional conduction the square cell was approximated as corner-less, with thicker walls to conserve thermal mass. Fig. 4 depicts the geometry and discretization scheme.

In each simulation, the brickwork begins at a uniform temperature, set at the designated peak temperature T_{peak}. Cold air at inlet temperature T_{in} is blown through the channel starting at a low flow rate, and heat conduction and convection are modeled from the firebrick to the air. Most air is fed through the bypass duct at the start of discharge to avoid delivering too much heat. However, the total mass flow rate through the brickwork and the bypass is always recombined before being sent to the application, so that the application always “sees” the same mass flow rate $\dot{m}_{op}$, operating temperature T_{op}, and discharge rate P_d (where $c_{p,air}$ is the specific heat capacity of air):

$$P_d = \dot{m}_{op} c_{p,air} (T_{op} - T_{in}) \tag{1}$$

Over the course of the discharge period the brickwork gradually cools down. Flow rate $\dot{m}_{air}$ through the brickwork is increased to maintain constant heat transfer. The increase in flow represents the redirection of flow from the bypass duct to the brickwork by actuation of dampers. The inlet and outlet temperatures of air are used to calculate the instantaneous discharge rate from the firebrick:

$$P_{inst} = \dot{m}_{air} c_{p,air} (T_{out} - T_{in}) \tag{2}$$

whenever P_{inst} falls slightly below P_d, the flow rate is slightly increased until $P_{inst} = P_d$. Eventually, T_{out} drops to T_{op}; beyond this point FIRES is too cold to deliver the desired T_{op}, and P_{inst} begins to fall below P_d. The simulation stops when $P_{inst} < P_d/8$.

The proper function of the simulation and validity of results was checked by running several simplified simulations and comparing them to analytical solutions, as well as one 3-dimensional CFD simulation. All of these cases were run with constant inlet velocity. Validation methods and results are included in supplementary Section 1.4.

3.1.1. Numerical scheme

The cell was discretized into uniform wall regions of width Δw, height Δh, and length $4a$ (where the factor four arises from taking the four walls as one region). Heat conduction was modeled using Fourier’s law. For simplicity and conservatism, especially with regard to thermal shock considerations, thermal conductivity was held constant at the lowest value over the temperature range.

$$q = -k_{FB} \frac{dT}{dx} \tag{3}$$

where k_{FB} is the firebrick thermal conductivity, q is the heat rate per unit area, and $\frac{dT}{dx}$ is the derivative of temperature in the direction of the brick width. With constant properties of firebrick, the heat flow into a small wall region of width Δw, height Δh, and length $4a$ over a short time period Δt can be approximated with the following relation:

$$\Delta Q_n = ((T_{n-1} - T_n) + (T_{n+1} - T_n)) \frac{k_{FB} 4a \Delta h \Delta t}{\Delta w} \tag{4}$$

where $4a\Delta h$ represents the area through which heat flows, and T is the temperature of the relative subscripted regions. Applying conservation of energy, the change in temperature ΔT_n of any region is related to the heat transferred ΔQ_n by:

$$\Delta Q_n = \Delta T_n * m_n c_n \tag{5}$$

where c_n is the specific heat capacity of the region material, and m_n is the mass of the region. In terms of the geometric parameters, the mass m_{FB} of each firebrick region, and the mass of the air channel region in the center of the cell, can be described as:

$$m_{FB} = \rho_{FB} \Delta w 4a \Delta h \tag{6}$$

and

$$m_{air} = \rho_{air} a^2 \Delta h \tag{7}$$

where ρ is the density, and FB denotes firebrick properties. By canceling terms and converting into matrix form, the change in temperature ΔT_n of any non-boundary region of firebrick during a time period Δt can be expressed as:

$$\Delta T_n = \begin{bmatrix} 1 & -2 & 1 \end{bmatrix} \begin{bmatrix} T_{n-1} \\ T_n \\ T_{n+1} \end{bmatrix} * \frac{k_{FB} \Delta t}{\rho_{FB} c_{FB} \Delta w^2} \tag{8}$$

Note that Eq. (8) is simply the heat equation described in finite difference form. This forms the basis for the tri-diagonal matrix with which to simulate the evolution of temperature for all non-boundary regions of the firebrick over time.

The boundary of the firebrick region at the outermost extremity of the cell, called region 1, is treated as an insulated boundary due to the symmetry of FIRES, such that no heat flows through. Because it only interacts with region 2, the temperature change of region 1, ΔT_1, is simply:

$$\Delta T_1 = \begin{bmatrix} -1 & 1 \end{bmatrix} \begin{bmatrix} T_1 \\ T_2 \end{bmatrix} * \frac{k_{FB} \Delta t}{\rho_{FB} c_{FB} \Delta w^2} \tag{9}$$

The temperature of the air region must also be included in the matrix, denoted as region N. This region is at the center of the cell. Heat flow into the region of firebrick that contacts the air, N − 1 (“N minus one”), is a mixture of conduction from the adjacent firebrick and convection from the air:

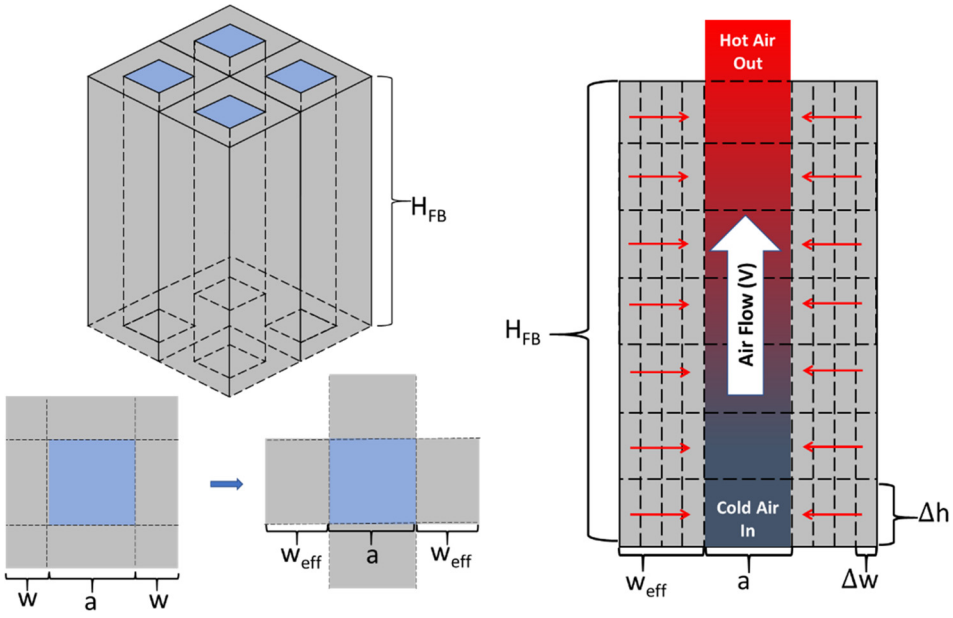

Fig. 4. Brickwork and "cell," corner-less approximation, and finite difference scheme along channel. The temperatures of the air and the laterally adjacent wall sections $\boldsymbol{\Delta w}$ determine the lateral heat transfer in the time step $\boldsymbol{\Delta t}$; the new temperatures for the discretized air and wall sections are calculated, and the column of air is stepped forward in time $\boldsymbol{\Delta t}$ by distance $\boldsymbol{\Delta h}$.

$$\Delta Q_{N-1} = (T_N - T_{N-1}) h_{air} 4a\Delta h\Delta t + (T_{N-2} - T_{N-1}) \frac{k_{FB} 4a\Delta h\Delta t}{\Delta w} \tag{10}$$

where h_{air} is the convective heat transfer coefficient. Lastly, the heat transfer into the air channel at the center of the cell, region N, comes only from convection from the firebrick region N-1, written as:

$$\Delta Q_N = (T_{N-1} - T_N) h_{air} 4a\Delta h\Delta t \tag{11}$$

Again, we can relate ΔQ_{N-1} and ΔQ_N to a change in temperature of the region by Eq. (5), with their respective mass terms in Eqs. (6) and (7), and manipulate them, resulting in two more matrix coefficients, for a total of three:

$$C_1 = \frac{k_{FB}}{\rho_{FB} c_{FB} \Delta w^2}; \; C_2 = \frac{h_{air}}{\rho_{FB} c_{FB} \Delta w}; \; C_3 = \frac{4h_{air}}{\rho_{air} c_{p,air} a} \tag{12}$$

Then the resulting thermal diffusion matrix takes the form:

$$\boldsymbol{C} = \begin{bmatrix} -C_1 & C_1 & 0 & 0 & \cdots & 0 & 0 \\ C_1 & -2C_1 & C_1 & 0 & \cdots & 0 & 0 \\ 0 & C_1 & -2C_1 & C_1 & \cdots & 0 & 0 \\ \vdots & \vdots & \ddots & \ddots & \ddots & \vdots & \vdots \\ 0 & 0 & \cdots & C_1 & -2C_1 & C_1 & 0 \\ 0 & 0 & \cdots & 0 & C_1 & -(C_1 + C_2) & C_2 \\ 0 & 0 & \cdots & 0 & 0 & C_3 & -C_3 \end{bmatrix} \tag{13}$$

The time evolution of temperature through the brickwork was solved using the Crank-Nicolson method, which takes the form:

$$(\boldsymbol{I} - \theta \boldsymbol{C}\Delta t)\boldsymbol{T_{new}} = (\boldsymbol{I} + (1-\theta)\boldsymbol{C}\Delta t)\boldsymbol{T_{old}} \tag{14}$$

where $\boldsymbol{I}$ is an identity matrix of equal dimensions to $\boldsymbol{C}$, $\boldsymbol{T}$ is the temperature matrix of the firebrick and air (before or after one time step Δt, denoted by subscript), and θ is the weighting factor between the implicit and explicit solution methods, which is set equal to 0.5 for the Crank-Nicolson scheme. Solving for $\boldsymbol{T_{new}}$ with this scheme yields a result that is second-order accurate in time and space [32].

The time step Δt was parameterized with the air inlet velocity V and the height step Δh:

$$\Delta t = \frac{\Delta h}{V} \tag{15}$$

such that all the heat transfer from the Δh region of firebrick is transferred to the mass of air that flows through Δh in the discrete time stepΔt. The resulting heat transfer matrix is applied at every height step Δh along the length of the channel at each time step Δt. The resulting temperature change in the $\Delta h * a^2$ column of air is passed to the next region of firebrick, and repeated until the cutoff heat output is reached.

The value of Δh was set by the number of vertical sections $N_{\Delta h}$, where $\Delta h = H_{FB}/N_{\Delta h}$, and the value of Δw was set by the number of firebrick width sections, $N_{\Delta w}$, related geometrically as $\Delta w = w_{eff}/N_{\Delta w}$. A finer mesh and smaller time step results in higher resolution and a higher computational cost. All simulations used $N_{\Delta w} = N_{\Delta h} = 10$, which was arrived at by testing for convergence of results on the base case. Compared to $N_{\Delta w} = N_{\Delta h} = 40$, all key performance parameters (explained in Section 3.2) of the base case were within 1–3%, with the exception of the spatially averaged peak temperature difference across firebrick ΔT_{avg}, which was within 10%. Given the other simplifying approximations and correlations used in this work, the results of the $N_{\Delta w} = N_{\Delta h} = 10$ mesh were considered acceptable for exploration of the design space and performance space.

3.1.2. Convective heat transfer correlations

Convection was modeled by calculating a convective heat transfer coefficient h_{air} at the interface of the firebrick and air using relations of Reynolds number $Re = \rho_{air} V D_h/\mu$, Prandtl number $Pr = c_{p,air}\mu/k_{air}$, and Nusselt number $Nu = h_{air} D_h/k_{air}$ that are valid for the operating temperature range (25 °C to 1700 °C), where V is the inlet air velocity, D_h is the hydraulic diameter, k_{air} is thermal conductivity, $c_{p,air}$ is the specific heat capacity, ρ_{air} is the density and μ is the dynamic viscosity of air. The Gnielinski relation [33] was used to calculate Nu from Re, Pr, and friction factor f.

$$Nu = \frac{\left(\frac{f}{8}\right)(Re - 1000)Pr}{1 + 12.7\left(\frac{f}{8}\right)^{0.5}\left(Pr^{\frac{2}{3}} - 1\right)} \tag{16}$$

For this relation fluid properties are evaluated at the bulk mean fluid temperature, $T_b = 1/2 * (T_{inlet} + T_{exit})$, with an accuracy of ± 20%. The Gnielinski relation is valid for $0.5 < Pr < 2000$, and $3000 < Re < 5 \times 10^6$, making it broadly applicable for FIRES's geometry and operating range, but is only accurate for smooth-walled channel flow. Rough channels can approximately double the heat

transfer rate to air. For heat transfer through rough channels, a slightly modified version of R. H. Norris' correlation [34] was used to calculate the factor by which roughness increases the Nusselt number compared to that of the smooth case:

$$\frac{Nu}{Nu_{sm}} = \begin{cases} \left(\frac{f}{f_{sm}}\right)^{\zeta} & for \ \frac{f}{f_{sm}} < 3 \\ 2 & for \ \frac{f}{f_{sm}} > 3 \end{cases} \tag{17}$$

where *sm* denotes values calculated with zero roughness, and ζ is a function of Prandtl number:

$$\zeta = 0.68Pr^{0.215} \tag{18}$$

The channel friction factor f was calculated by the S.E. Haaland relation [35]:

$$f = \frac{1}{\left(-1.8\log_{10}\left(\frac{6.9}{Re} + \left(\frac{E}{3.7D_h}\right)^{1.11}\right)\right)^2} \tag{19}$$

where the surface roughness E is a measure of the root mean square (RMS) height of bumps or depressions in the wall surface and the hydraulic diameter is calculated as $D_h = 4FlowArea/Perimeter$. The S.E. Haaland relation is a close approximation (± 2%) of the commonly used Colebrook equation for surface roughness, which is itself usually considered to be accurate to ± 15% [35]. Because friction factor is a function of the surface roughness E as well as Re the optimal roughness design of the brick channels depends on the expected flow rates of the application. Fig. 5 shows the roughness-induced heat transfer improvement factor as a function of both relative roughness (E/D_h) and Re.

All of the previous relations and corrections discussed assume a relatively small difference in temperature between the bulk fluid and the channel surface. When this temperature difference is non-negligible, it is common to use a Sieder-Tate type correction for Nu and f to address the large differences in fluid properties near the wall compared to the bulk fluid temperature. At each of the discrete regions Δh during every time step Δt, the following corrections were used:

$$\frac{Nu}{Nu_b} = \left(\frac{T_{surface}}{T_{air}}\right)^n \quad \text{and} \quad \frac{f}{f_b} = \left(\frac{T_{surface}}{T_{air}}\right)^m \tag{20}$$

where b denotes values calculated at bulk fluid properties, $T_{surface}$ and T_{air} denote local temperatures of the air and outermost wall section at each Δh region, and m and n are exponents whose values depend on turbulent or laminar flow, and are prescribed by Mills [36] as:

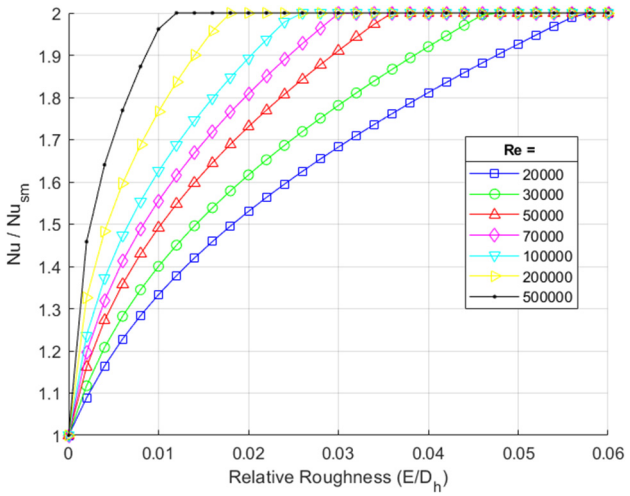

Fig. 5. Roughness-induced heat transfer improvement factor (Norris relation).

$$n = \begin{cases} 0 & if \ laminar \\ -0.55 & if \ turbulent \end{cases} \text{ and } m = \begin{cases} 1 & if \ laminar \\ -0.2 & if \ turbulent \end{cases} \tag{21}$$

Pressure drop through the heated air channel [37] was calculated as the sum of the frictional losses, gravity losses and acceleration losses. The pressure drop at each time step Δt at each discretized length of the channel Δh was summed, where G, the mass flux, is constant along the channel:

$$p_{drop} = \left[\sum_{I=1}^{N_{\Delta h}} \left(f\frac{\Delta h}{D_h}\frac{G^2}{2\rho_{air,I}} + \rho_{air_I} * g * \Delta h\right)\right] + G^2\left(\frac{1}{\rho_{air,out}} - \frac{1}{\rho_{air,in}}\right) \tag{22}$$

In all cases flow was assumed to be upwards, but the gravity contribution to pressure is small such that results are generalizable to other flow directions. Pressure losses upstream or downstream of the brickwork are not included herein.

3.2. Discharge performance characteristics

The discharge performance of FIRES can be evaluated in several ways, the merits of which depend on the application. The key performance characteristics of interest are as follows:

- **Nominal discharge-rate-to-storage-capacity ratio (DQR)**[1]**:** The ratio of FIRES's discharge rate P_d and storage capacity Q_s, referred to herein as DQR, represents the fraction of capacity depleted from FIRES per hour (MW/MWh). A higher DQR means a more rapid discharge period and improved flexibility for responding to changes in energy markets.
- **Discharge fraction at constant power (DF_p):** The DF_p represents the fraction of FIRES's total stored energy that can be discharged at the desired discharge rate and temperature. A higher DF_p means a longer period of constant nominal discharge and less dependence on backup heat.
- **Volumetric fraction of firebrick ($F_{v,FB}$):** A larger volume of firebrick relative to air reduces system size by increasing overall energy density.
- **Required fan power (P_{fan}):** A lower P_{fan} value places lesser requirements on the blower system.
- **Spatially averaged peak temperature difference across firebrick (ΔT_{avg}):** A lower ΔT_{avg} reduces thermal stresses in the firebrick during discharge and lowers risk of fatigue cracking.

FIRES can be optimized according to the priorities of the application. For example, systems with pressure vessels or other size constraints may prioritize $F_{v,FB,}$ and systems without backup heat will maximize DF_p. Simulations were focused on determining the relative tradeoffs between each performance characteristic.

3.3. Base case

As a starting point of analysis, a "base case" FIRES unit is analyzed and discussed in detail to serve as reference for the rest of the discussion. Table 2 shows the base case parameters and summary of simulation results. The base case set of parameters was chosen to represent a low-tech (i.e. low-temperature, low-pressure) FIRES unit that may operate with inexpensive metallic heaters (1200 °C) and comfortably provide heat for industrial sectors that do not require heat above 500 °C, including various types of food preparation, chemical production, distillation and drying [29]. The base case is an alumina system

[1] The DQR is emphasized as a nominal value because in practice FIRES units will not discharge at their nominal rate throughout the discharge period. An "effective" DQR, or DQR_{eff}, can be defined for a full discharge period of FIRES by taking the inverse of the time needed to fully deplete the unit.

Table 2
Base case inputs, derived parameters and results summary of FIRES discharge simulation.

Input design parameters for discharge calculations				
Design parameter	Symbol	Unit	Value	Note
Material	–	–	Al_2O_3	
Air pressure	P_{air}	kPa	101.3	
Air inlet temperature	T_{in}	°C	30	
Peak storage temperature	T_{peak}	°C	1200	
Minimum storage temperature	T_{min}	°C	100	Nominal minimum temperature at which firebrick is considered depleted (above T_{in})
Application operating temperature	T_{op}	°C	500	
Heat storage capacity	Q_s	MWh	250	
Nominal discharge rate	P_d	MW	50	
Nominal height-to-diameter ratio	HDR	–	5	Considers a solid cylinder of firebrick before taking into account air channel volume
Air channel width	a	m	0.1	
Firebrick wall half-width	w	m	0.05	Half-width of firebrick that forms air channels
Firebrick surface roughness	E	mm	3.045	
Derived equivalent parameters				
Derived parameter	Symbol	Unit	Value	Notes
Required volume of firebrick	V_{FB}	m^3	177	Constrained by Q_s, $T_{peak} - T_{min}$, and material (does not include air volume)
Volumetric fraction of firebrick	$F_{v,FB}$	–	0.75	$1 - [a^2/(a + 2w)^2]$
Total brickwork volume	V_{total}	m^3	233	$V_{FB}/F_{v,FB}$ (includes air volume)
Nominal diameter	D_{FB}	m	3.5	$[(4V_{FB})/(HDR * \pi)]\hat{}(1/3)$ (does not include air volume)
True diameter	D_{true}	m	4.1	$D_{FB}/(F_{v,FB})\hat{}(1/2)$ (includes air volume)
Height	H_{FB}	m	18	$D_{FB} * HDR$
Cell width	w_{cell}	m	0.2	$a + 2w$
Number of cells	N_{cell}	–	323	Constrained by V_{FB}, w_{cell} and $F_{v,FB}$
Nominal discharge rate to storage capacity ratio	DQR	h^{-1}	0.2	P_d/Q_s
Results summary				
Result	Symbol	Unit	Value	Notes
Discharge fraction at constant power	DF_p	–	0.67	Fraction of stored energy Q_s that was discharged at the nominal rate P_d
Peak pressure loss	Δp_{max}	kPa	9.19	
Required fan power	P_{fan}	kW	810	
Peak firebrick temperature difference	ΔT_{max}	°C	196	
Spatially-averaged peak firebrick temperature difference	ΔT_{avg}	°C	155	

with capacity 250 MWh and a DQR of 0.2 h^{-1}, i.e. a discharge rate of 50 MW, and a nominal discharge time of 5 h. For all subsequent cases it should be assumed that any unspecified parameters are the same as the base case.

Fig. 6 shows the behavior of the base case FIRES unit during the simulated discharge period. The outlet temperature of air (Fig. 6a) gradually decreases in time as the brickwork cools down. As previously described, flow rate through the brickwork is increased throughout this period to maintain a constant discharge rate (Fig. 6b) for as long as possible. As flow rate is increased, a sharp increase in fan power (Fig. 6c) also occurs, since $P_{fan} \propto (flow\ rate)^3$. After approximately 200 min, the outlet temperature of the brickwork drops below the application operating temperature of 500 °C, and the discharge rate drops below 50 MW. The 200 min of constant discharge corresponds to a DF_p of 0.67; that is, 67% of FIRES's stored heat was discharged at the desired power and temperature. Beyond this point, fossil fuel heating would be required to maintain the desired operating conditions. Fan power peaks at 810 kW, or 1.6% of the heat discharge rate.

Fig. 6d shows the time evolution of temperature difference between the firebrick wall centerline and surface at different channel locations. The temperature difference across the firebrick wall is of concern when considering the threat of thermal shock in different designs. The largest temperature difference ΔT_{max} is developed rapidly at the channel inlet where 30 °C air is exposed to 1200 °C firebrick. Subsequent portions of firebrick experience a peak of reduced magnitude because the airstream has been warmed by the previous sections. Note that the high value of ΔT_{max} seen in the simulation (196 °C in the base case) is avoidable in practice, either by maintaining a colder inlet region or having a preheating chamber upstream of the hot brickwork. A more appropriate metric for examining thermal shock in a design is the *spatially averaged* peak temperature difference along the channel, ΔT_{avg} (155 °C in the base case). Thermal shock considerations are discussed further in Section 3.6.

3.4. FIRES discharge design space

FIRES's design parameters and operating conditions were varied to map its performance over the option space. All units analyzed have a heat storage capacity Q_s of 250 MWh and peak temperature T_{peak} of either 1200 °C or 1550 °C, which were chosen in accordance with reasonable capabilities of Fe-Cr-Al and SiC heaters, respectively. The remaining key design parameters of FIRES were split into two categories: those that may be changed without altering FIRES's overall size and shape (discharge-to-storage ratio DQR and cell width w_{cell}) , and those that determine the overall system size and shape (the height-to-diameter ratio *HDR* and volume fraction of firebrick $F_{v,FB}$). Those results are shown in Fig. 7 and Fig. 8 respectively. Both figures show the discharge fraction at constant power DF_P and the relative fan power requirements of a variety of designs plotted against operating temperature T_{op}.

When analyzing the effect of firebrick channel dimensions, it is most useful to discuss $F_{v,FB}$ and w_{cell}, which are parameters derived from the air channel width a and firebrick wall half-width w (Table 2). These parameters are preferred because individual values of a and w are not very meaningful independent of one another. On the other hand, $F_{v,FB}$ is of interest with respect to energy density, and describes the ratio of a and w. When $F_{v,FB}$ is fixed, w_{cell} can be changed to explore the heat transfer performance and fan power penalty of smaller cells without

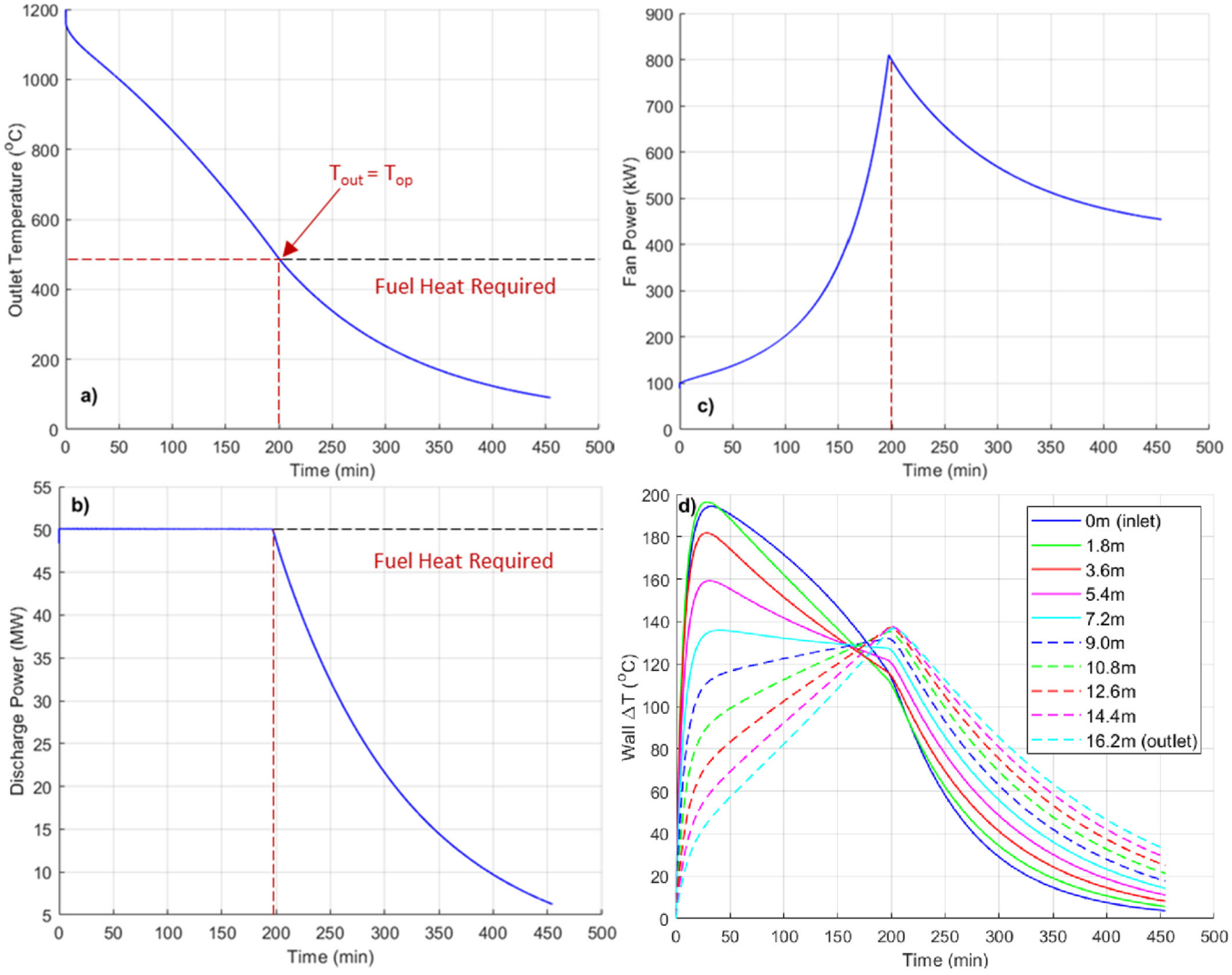

Fig. 6. Base case discharge results. (a): Air outlet temperature versus time; (b): Discharge rate versus time; (c): Fan power versus time; (d): Temperature difference across the firebrick wall versus time at different equally spaced channel locations.

altering energy density, cross-sectional flow area, or overall system size.

In all cases, applications with lower operating temperatures T_{op} can maintain a longer period of constant discharge. For T_{op} of 500 °C all designs have a DF_P between 0.60 and 0.90 with little sensitivity to T_{peak}, suggesting that SiC or $MoSi_2$ heaters are likely not warranted at lower T_{op}. This however changes when applications require higher temperatures; at T_{op} = 1100 °C, the difference in DF_P between the 1550 °C and 1200 °C systems is generally 0.20, i.e. 20% more of the stored energy is discharged at the desired operating conditions, making the system with higher T_{peak} significantly less dependent on fossil fuel backup.

Operating FIRES at higher discharge rates, i.e. higher DQR, decreases DF_P because convective heat transfer improves less than linearly with the increased flow rate. Increasing DQR also dramatically increases the required fan power because an increase in DQR requires a proportional increase in flow rate. Fan power requirements may be lowered in exchange for a slightly lower DF_P by limiting the flow through FIRES, which is essentially the same as operating FIRES for a higher T_{op}.

Since most applications are expected to operate on daily cycles or longer ($DQR < 0.125\,h^{-1}$), results suggest that FIRES can comfortably accommodate most energy markets, and may be capable of effectively capturing and discharging cheap electricity in time periods of a few hours for flexible response to changes in renewable generation.

A smaller w_{cell} substantially benefits heat transfer and results in a higher DF_P, even at high DQR and high T_{op}, with only moderate fan power penalty. This arises from the higher specific surface area of firebrick, which causes a rise in pressure drop but also demands less flow rate. Results suggest that FIRES designed with thin firebrick walls and many air channels may reliably discharge 90% of stored heat at the desired temperature, without fossil fuel backup. The minimum w_{cell} is not immediately clear, but will be limited by practical manufacturing and construction techniques. Dimensions used herein were found to be in class with existing chimney-style bricks.

An increase in *HDR* is shown to increase both DF_P and fan power, arising from the constriction of flow area and lengthening of flow path. Higher T_{op} applications favor larger *HDR*, where the DF_P advantage is greatest and fan power penalties are reduced.

An increase in $F_{v,FB}$ improves energy density but dramatically increases fan power requirements. $F_{v,FB}$ values between 0.7 and 0.8 are generally reasonable, which is consistent with the dimensions of commercially available chimney bricks like those shown in Fig. 1. With respect to DF_P, the optimal $F_{v,FB}$ depends on T_{op}. At higher flow rates, the improved convective heat transfer coefficient of excessively high $F_{v,FB}$ becomes outweighed by the higher brickwork thermal resistance, causing a drop in DF_P despite the large fan power penalty.

So far all results have been presented for a system with a capacity of 250 MWh. However, results are generalizable to any FIRES system that is built from the same unit cell, so long as the materials properties, T_{in}

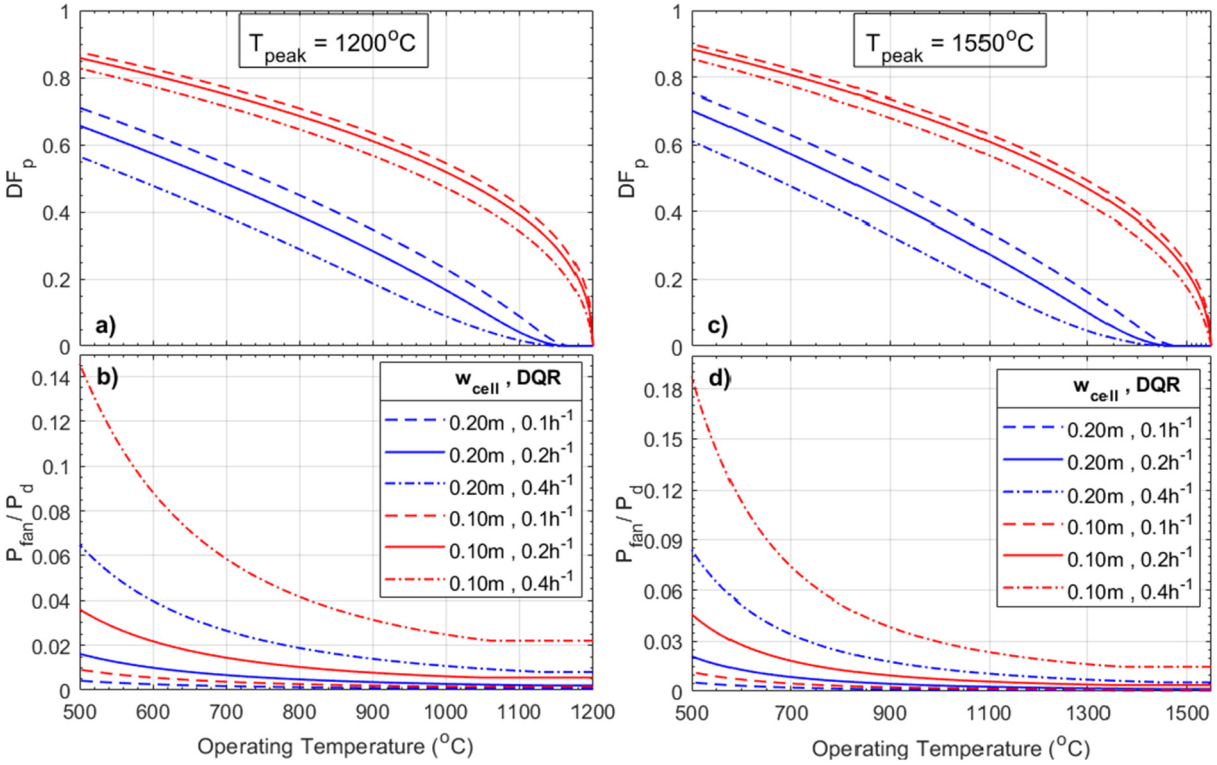

Fig. 7. Performance map of DF_P and fan power as a function of DQR, and w_{cell}. All units are alumina, with Q_s = 250 MWh, HDR = 5, and $F_{v,FB}$ = 0.75. (a): DF_P, with T_{peak} = 1200 °C. (b): P_{fan}/P_d, with T_{peak} = 1200 °C (c): DF_P, with T_{peak} = 1550 °C. d): P_{fan}/P_d, with T_{peak} = 1550 °C.

and T_{peak} are also the same. This arises from the fact that the brickwork is a repeated cell geometry. When the cell dimensions (w_{cell} $F_{v,FB}$ and H_{FB}) are identical in two systems, the capacity difference between them is simply a difference in the number of parallel cells in the brickwork. It can be shown geometrically that the height H_{FB} of two systems is the same when the following relation involving HDR and Q_s is satisfied, in which case their performance curves are identical for a given DQR:

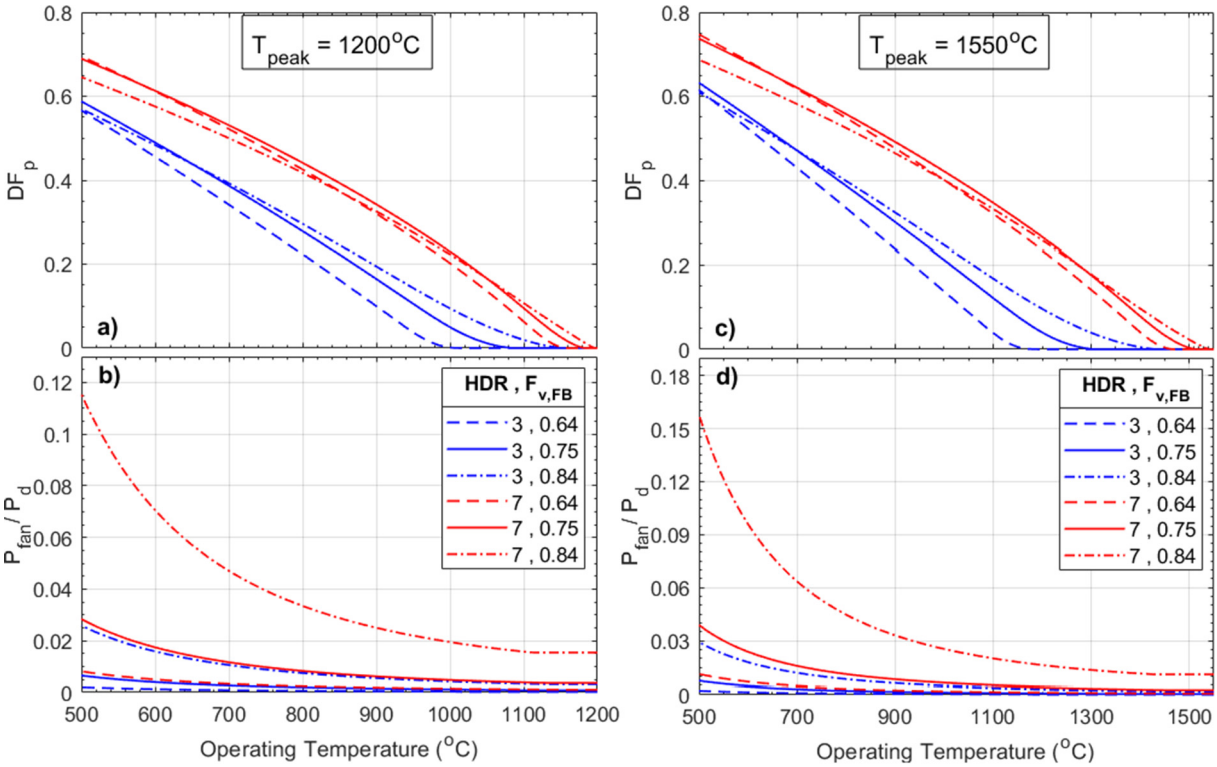

Fig. 8. Performance map of DF_P and fan power as a function of HDR, and $F_{v,FB}$All units are alumina, with Q_s = 250 MWh, DQR = 0.2 h^{-1}, and w_{cell} = 0.20 m. (a): DF_P, with T_{peak} = 1200 °C. (b): P_{fan}/P_d, with T_{peak} = 1200 °C. (c): DF_P, with T_{peak} = 1550 °C. (d): P_{fan}/P_d, with T_{peak} = 1550 °C.

$$\sqrt{Q_{s1}}\,HDR_1 = \sqrt{Q_{s2}}\,HDR_2 \quad (23)$$

When Eq. (23) is applied to the curves in Fig. 7, it can be understood that they apply equally to systems of 500 MWh and *HDR* of 3.5, or 1000 MWh and *HDR* of 2.5, etc. The practical implication is that the height of the brickwork is set to meet a specific set of performance requirements and the diameter is set to obtain the desired capacity. For greater capacities, the decision to build one large FIRES vessel or multiple parallel FIRES vessels will depend on the associated cost of each option.

Results for silicon carbide FIRES units, which can be found in the supplementary section (1.2, Fig. 14), exhibit the same general behaviors as the alumina units discussed herein, but differ from alumina in two noteworthy ways: (1) DF_p is increased considerably, due to the higher thermal conductivity of silicon carbide; (2) fan power is reduced, due to lower energy density of silicon carbide, which results in a larger system and larger relative flow area than alumina for the same *HDR*. Magnesia units, not included here, behave similarly to alumina units.

3.5. High pressure case: FIRES coupled with gas turbine

FIRES heat storage has the unique potential to be incorporated within the pressure boundary of gas turbine power cycles to partly replace the burning of fossil fuels or augment the performance of generation-IV nuclear or CSP plants. One candidate configuration is examined herein but results will be similar for other gas turbines.

FIRES coupled with a nuclear air-Brayton combined cycle, NACC, receives air that has already been compressed and heated by a generation-IV nuclear reactor, and further heats the air before expanding it through the turbine in order to increase power output. FIRES designs were simulated with air inlet conditions of 1000 kPa and 670 °C, and operating temperature T_{op} of 1065 °C. These conditions produce approximately 66% round-trip efficiency in the NACC, and are similar to a NGCC operating with an efficiency in the mid-50% range. The designs considered were all silicon carbide firebrick, with storage capacity Q_s of 1500 MWh and discharge rate P_d of 214 MW (DQR of 0.142 h^{-1}). Fig. 9 shows results for T_{peak} values of 1500 °C and 1700 °C, which correspond to capabilities of SiC and $MoSi_2$ heaters respectively. *HDRs* of 3 and 5 were tested. $F_{v,FB}$ and w_{cell} were kept constant at 0.75 and 0.20 m.

The DF_p of FIRES units coupled with the NACC at peak temperatures of 1500 °C and 1700 °C ranged from 0.77 and 0.85, respectively. Most notably, the high-pressure systems have fan power requirements of only 100 s of kilowatts, similar to smaller low-pressure systems, despite the significantly larger system size and comparable DQR. The largest fan power fraction P_{fan}/P_d of the high-pressure cases is only 0.3%, compared to 1.4% in the low-pressure base case. This fan power advantage is a result of the greater air density at turbine pressures, and grants FIRES units coupled to power cycles more freedom in *HDR* and $F_{v,FB}$ for optimal vessel designs with less of a fan power penalty.

3.6. Thermal shock considerations

The temperature differences that form across the firebrick walls in different FIRES designs during operation must be compared to the thermal shock resistance of the candidate firebrick materials to avoid cracking. Although not an exact metric, ΔT_{avg} serves as a figure of merit by which to compare the relative threat of cracking for different designs and materials. Fig. 10 shows ΔT_{avg} for various FIRES designs during discharge, as well as the approximate cold shock temperature limits ΔT_{limit} of firebrick candidates. The wide ranges of ΔT_{limit} shown for alumina (~40–400 °C) and silicon carbide (~80–420 °C) arise from the wide range in properties of bulk commercial ceramics, especially tensile strength. It is noteworthy that ΔT_{limit} of *hot shock* is a factor 3.2 larger than cold shock, which means charge rates are less constrained by ΔT_{limit} than discharge rates.

ΔT_{avg} is driven upward by increasing DQR, *HDR*, $F_{v,FB}$, and T_{peak}. Most alumina cases discussed fall within the range of ΔT_{limit} of alumina, such that alumina with sufficiently high tensile strength may be used to avoid cracking, but designs with higher ΔT_{avg} will be more susceptible to fatigue cracking from thermal cycling[2]. Units with small w_{cell} experience greatly reduced ΔT_{avg} even at high DQR and high T_{peak}, suggesting once again that w_{cell} should be minimized for best performance. Alternatively, silicon carbide is an attractive option in high performance designs (high T_{peak}, DQR, $\sqrt{Q_s}HDR$, etc.) owed mostly to its higher thermal conductivity at elevated temperature.

4. Charge

Off-the-shelf metallic heaters are expected to charge FIRES in near-term deployment. Charging periods were simulated for the base case FIRES unit (Table 2) to determine the practicality of achieving relatively fast charge rates with metallic heaters at different charge-rate-to-storage-capacity ratios (CQR). Heat transfer from resistance heaters to firebrick was modeled with finite difference methods similar to those used in discharge modeling. Unlike discharge, the charge process is dominated by radiative heat transfer between the brickwork and the integrated heaters, whose wattage can be controlled to the desired output so long as it is within recommended limits. Charge was therefore modeled purely as conduction through the firebrick with a constant uniform heat flux at the channel surface, representative of metallic heater wires running along the channel walls. The problem simplifies to one discretized firebrick slab (four symmetrical walls with no height dependence) of thickness w_{eff} discretized into Δw sections. The boundary condition for constant heat flux was input as:

$$\Delta T_N = \begin{bmatrix} 1 & -1 \end{bmatrix} \begin{bmatrix} T_{N-1} \\ T_N \end{bmatrix} * \frac{k_{FB}\Delta t}{\rho_{FB} c_{FB} \Delta w^2} + \frac{q^{''}\Delta t}{\rho_{FB} c_{FB} \Delta w} \quad (24)$$

where region N of the firebrick is the section exposed to the heat flux of the metallic heaters, and $q^{''}$ is the heat flux the firebrick experiences, expressed as $q^{''} = P_c/(4aH_{FB}N_{cell})$. Convergence was found at $N_{\Delta w} = 40$, with less than 1% change for higher values.

Charge simulations began with the firebrick wall at the nominal minimum temperature of the system T_{min}, and ended when firebrick the surface reached the peak temperature T_{peak}, 1200 °C in the base case.

The base case FIRES unit was simulated with a CQR of 0.2, 0.3, 0.4, and 0.5 h^{-1}. The resulting temperature difference ΔT_{avg} was 138 °C, 207 °C, 276 °C, and 345 °C, respectively. This is within the hot shock ΔT_{limit} range of alumina (~128–1280 °C). The necessary amount of heater wire to achieve a CQR of 0.3 h^{-1} was estimated considering the largest standard stock diameter (1 cm) of Kanthal APM™ wire [26] operating at a constant 40 kW/m^2 surface loading throughout operation. The heating required may be provided with approximately ten vertical wires per channel, equal to 58,000 m long and 33.4 metric tons. A CQR of 0.3 h^{-1} represents a charge time of only 3.3 h, significantly faster than the charge rate required for daily cycling; results support the expectation that metallic heaters can reasonably heat FIRES operating on daily cycles or shorter. For more details of charge results, refer to supplementary section 1.2.

The mass of heater wire may be reduced by using a smaller wire diameter to increase relative surface area, or by operating at a higher surface loading. These modifications generally decrease the expected lifespan of the heaters. The optimal tradeoff between diameter, surface load and required wire length may be informed by industrial heating best practices.

5. Insulation

FIRES insulation will be designed by determining the lowest practically achievable leakage rate with respect to charge and discharge

[2] The ΔT_{limit} of alumina for surviving "infinite fatigue," or 10^7 cycles, is approximately 15°C – 65°C [38].

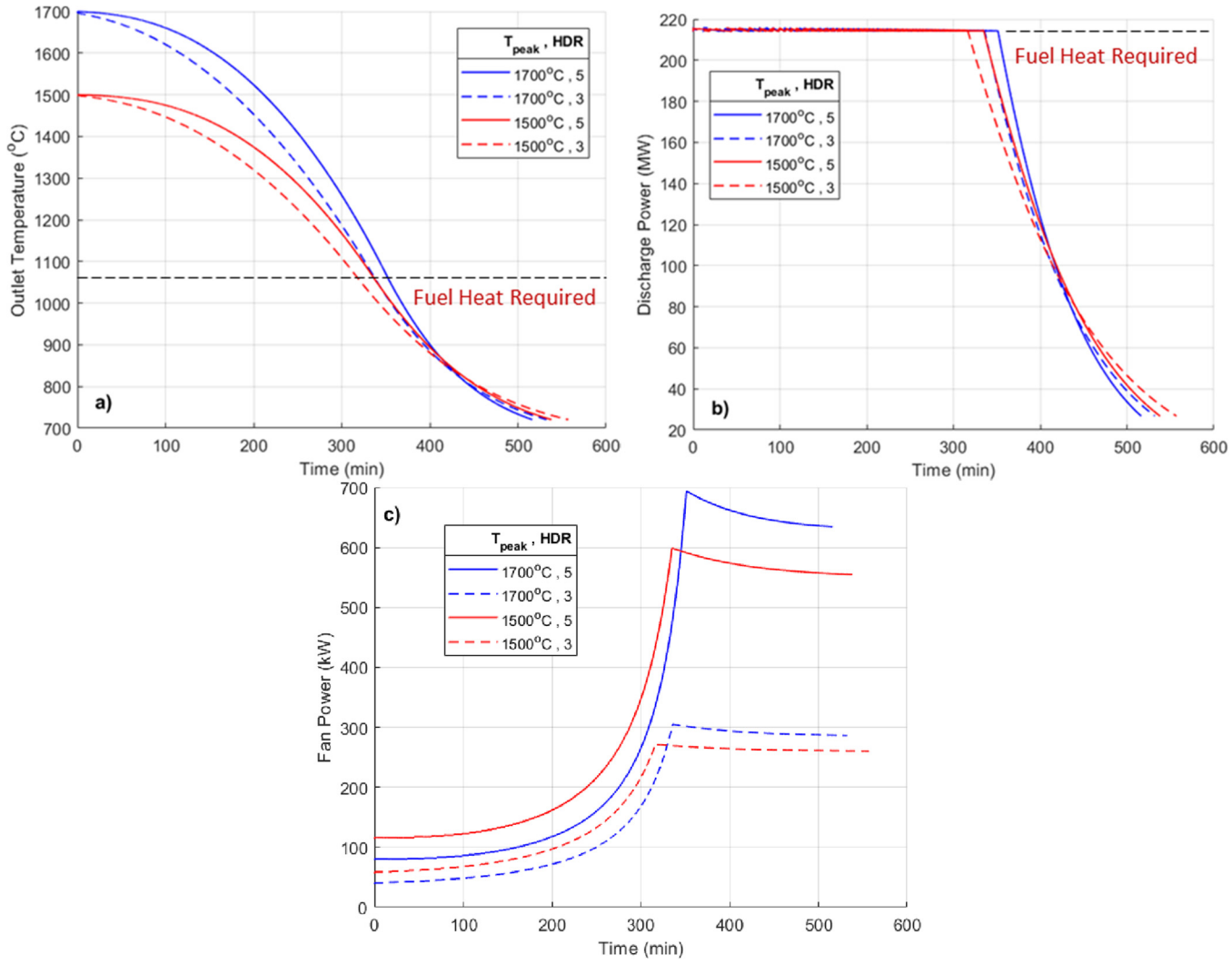

Fig. 9. Discharge results for FIRES designs under sample NACC conditions. Silicon carbide, Pressure = 1000 kPa, Q_s = 1500 MWh, P_d = 214 MW. $F_{v,FB}$ = 0.75, w_{cell} = 0.20 m. (a): Outlet temperature versus time; (b): Discharge rate versus time; (c): Fan power versus time.

cycles, space constraints and cost. Preliminary heat leakage calculations were used to determine the thickness of insulation for the desired period of heat storage. The geometry to be insulated was taken as a cylinder of overall brickwork diameter D_{true} and height H_{FB}, where the surfaces to be insulated are the top, bottom, and circumference. Heat leakage was calculated through one or two layers of insulation with peak temperature limits suitable for FIRES's peak temperature. Heat leakage through the insulation was modeled as steady state and 1D:

$$P_{Leak} = k_{INS,n}(2A_c)\frac{\Delta T_n}{w_{INS,n}} + k_{INS,I}2\pi H_{FB}\frac{\Delta T_n}{\ln\left(\frac{D_{inner,n}+2w_{INS,n}}{D_{inner,n}}\right)} \quad (25)$$

P_{Leak} is the leakage rate of heat through the insulation, $w_{INS,I}$ is the thickness of the insulation layer, k_{INS} is the bulk average thermal conductivity of the insulation, ΔT_n is the temperature difference across the *nth* insulation layer, $D_{inner,n}$ is the inner diameter of the cylindrical shell of insulation that wraps around the cylinder, and A_C is the cross sectional area of the cylinder. Eq. (25) is composed of two terms: conduction through the top and bottom walls of the cylinder, modeled as conduction through a slab, and conduction through the circumferential area of the cylinder. The outer wall was set to 50 °C, and the best value of k_{INS} available among firebrick insulation (from [46]) was used in each case.

The base case FIRES unit, a 250 MWh system with peak temperature of 1200 °C, can retain 90% of its heat for 2 days (5% leakage per day) with a 3.1% volume increase, or 8 days (1.25% leakage per day) with a 14.5% volume increase. Although this analysis does not take into account penetrations from the electrical heating system, results are promising for storage periods on the order of a week or more. These leakage rates are in class with those of thermal energy storage systems used in CSP plants, which are reasonably kept to 3–5% leakage per day [9,39]. Systems of higher T_{peak} can achieve similarly low leakage rates with more insulation. Larger capacity systems may store longer due to their smaller surface-area-to-volume ratio. Table 5 in Section 1.5 of the supplement shows more results.

The results herein consider conventional insulation; however, dynamic insulation may dramatically lower heat losses depending upon the cycle operation. There is the option of including air channels in the outer half of the insulation. During discharge, the incoming airstream may first be fed through these channels and preheated by the warm insulation. This recovers heat that would have ultimately been lost. For a FIRES unit on a daily cycle, this can result in very low heat losses.

6. Preliminary economic evaluation

FIRES economics are evaluated with respect to cost estimates based on the base case design and a market analysis of a small characteristic system deployed in northwestern Iowa.

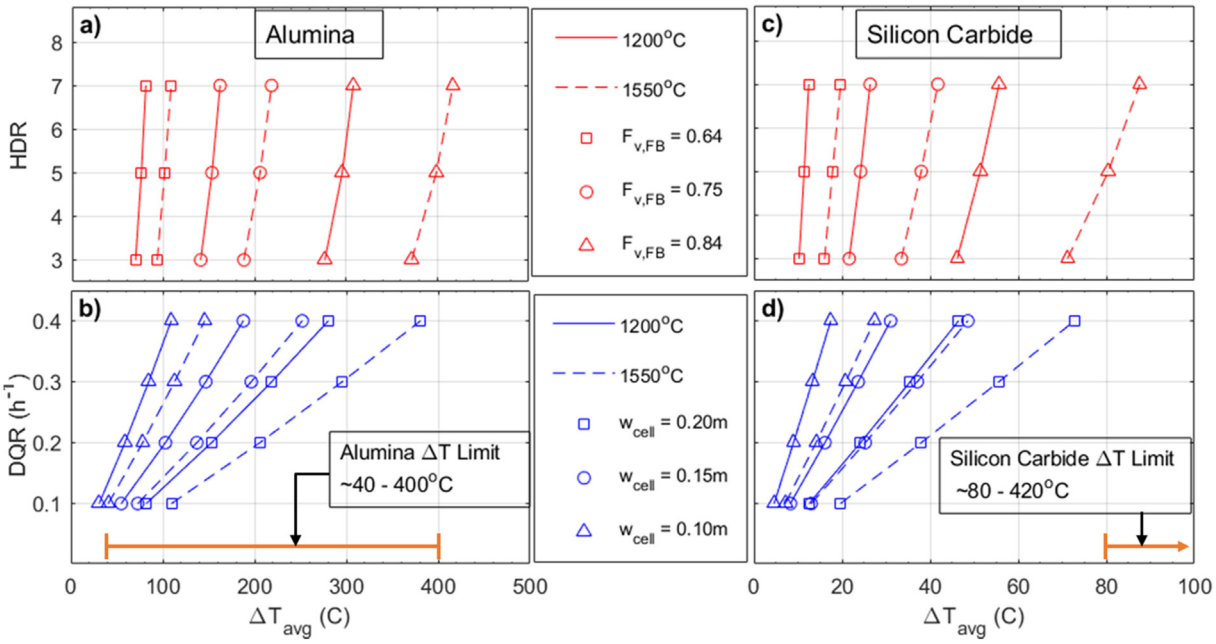

Fig. 10. Spatially averaged peak temperature difference across firebrick ΔT_{avg} for various FIRES designs. In all cases Q_s = 250 MWh. Systems are alumina (a, b) or silicon carbide (c, d). Variations of *HDR* and $F_{v,FB}$ (a, c) have constant DQR = 0.2 h^{-1} and w_{cell} = 0.20 m. Variations of DQR and w_{cell} (b, d) have constant *HDR* = 5 and $F_{v,FB}$ = 0.75. For comparison the range of cold shock temperature limits of alumina and silicon carbide are shown on the temperature axis, reported by Lu and Fleck (Original result reported as the "maximum temperature jump," $T_i - T_\infty$, sustainable by a slab of uniform temperature T_i exposed to air of T_∞, with a Biot Number $Bi = \infty$. When $Bi = \infty$ the temperature of the slab at the air interface equals T_∞ upon exposure, such that $(T_i - T_\infty) = (T_{outer} - T_{inner})_{max}$) [38].

6.1. Cost estimates

Table 3 shows a breakdown of estimated costs for the key components of the base case FIRES system based on cost functions from literature and online vendor prices. These components include the firebrick, insulation, blower, containment vessel, metallic heater wire, and step-down power transformer. Costs are for components and materials that are as close as possible to the simulated base case, but not exact. Cost estimates have wide uncertainties due to the many case-specific circumstances that cannot be easily modeled. Nonetheless the estimates herein are useful for characterizing the cost of FIRES with respect to other storage technologies.

Cost estimates of the vessel and blower were made using relations from Brown [40]. Costs are a function of volumetric capacities, in the units of gallons and cubic feet per minute (cfm), and pressure in the units of psig:

$$\$vessel_{2005} = 5180\left(\frac{gallons}{1000}\right)^{0.67} * (0.0023 Pressure_{psig} + 0.66) \quad (26)$$

$$\$blower_{2005} = \begin{cases} 66(cfm)^{0.63} & for \;\; 1 \;\; psig \\ 23(cfm)^{0.82} & for \;\; 3 \;\; psig \end{cases} \quad (27)$$

For base case cost estimation, a vessel pressure of 15 psig and blower pressure of 1 psig was used (close to the base case Δp_{max},1.3 psig). The Chemical Engineering Plant Cost Index (CEPCI) was used to bring equipment costs from the year 2005 (CEPCI = 460) to 2017 values (CEPCI = 567.5). Average install factors of 1.72 and 1.42 were used for vessel and blower installation respectively, as reported in [41].

Transformer purchase cost was estimated from [42] with a reported installation factor of approximately 1.3. The base case uses a 3-phase 75 MW_e step-down transformer (115–13.8 kV).

Values for firebrick and heater wire were estimated from online vendors. checker bricks like those shown in Fig. 1 were typically quoted between $100/ton and $500/ton at a variety of alumina contents, with the remaining composition typically made up by silica. The highest alumina contents (≥80%) were taken as $500/ton and was used for estimation. Since insulating firebrick is also typically composed of silica and alumina, the insulation price was also taken as $500/ton. Fe-Cr-Al wire with maximum continuous temperatures of 1400 °C or 1425 °C were typically quoted between $3/kg and $10/kg, with minimum orders varying from 5 kg to 1 ton, and vendor supply abilities of 200–500 tons/month. $5/kg was used for heater wire cost estimation.

The installation factors of the firebrick, insulation and heaters depend on the manufacturing strategy of FIRES. Previous firebrick E-TES

Table 3
Summary of FIRES cost estimates.

Cost estimates for characteristic FIRES unit (250 MWh, 75 MW_e, 50 MW_t)							
Key components –	Purchase cost $	Install factor	Installed cost	Break-down %	Cost per unit charge $/kW	Cost per unit discharge $/kW	Cost per unit storage $/kWh
Firebrick	353,000	1.50	529,500	18.4	7.06	10.59	2.12
Insulation	31,064	1.50	46,596	1.6	0.62	0.93	0.19
Transformer	1,000,000	1.30	1,300,000	52.2	17.33	26.00	5.20
Blower	227,700	1.42	323,334	11.9	4.31	6.47	1.29
Containment vessel	137,700	1.72	236,844	7.2	3.16	4.74	0.95
Metallic heater wire	167,000	1.50	250,500	8.7	3.34	5.01	1.00
Unit total	1,916,464	1.40	2,686,774	100	35.82	53.74	**10.75**

systems were sold as a prefabricated insulated box with firebrick and heaters already integrated. The modularity of FIRES designs will likely have a large impact on installation cost. Additional general considerations are the case-specific logistics of coupling to different facilities with different site layouts, which may require more or less additional ductwork, electrical lines, etc. In the present study, an installation factor of 1.5 was chosen for the firebrick and heater wire.

In total, the base case component system cost is estimated as $1,916,400, or $7.67/kWh, and the installed cost is $10.75/kWh. Despite the uncertainty of the installation factors, which vary widely between individual projects, the $10.75/kWh result is as an attractive baseline that accentuates the low cost of TES compared to that of other electricity storage technologies, $250–$500/kWh batteries [5].

Individual performance aspects of FIRES may be adjusted without dramatically affecting the overall cost. The firebrick and containment represent 26% of cost, such that a doubling of storage capacity would only mildly increase overall cost, while driving the cost per kilowatt-hour down significantly. The cost curves of containment and insulation both favor larger capacity. Likewise, extra insulation (1.6% of cost) may be added inexpensively outside of the containment for longer storage periods. The discharge rate may be increased with a larger blower so long as the power requirements are not prohibitively high, which is tied to the geometry of the system. Charging power may be increased by adding more heater wire (8.7% of cost), so long as the electrical system supports greater charge rates. Alternatively, operating at the same charge rate with more wire allows for a lower average wattage loading and less frequent replacement.

All component cost curves indicate improved economics when scaling FIRES to greater storage capacities, including the transformer. In the regime of the base case, the 75 MW_e transformer (52% of cost) is the dominant cost of system, with a unit power purchase cost of $13.33/$kW_e$. Larger transformers in the 100 s of MW cost less than $10/$kW_e$ [42]. conversely, the economic case for FIRES is weakened at lower transformer ratings, unless FIRES's charge rate is small enough to avoid a transformer entirely and be powered by the capacity of the existing power system (as is the case for existing firebrick E-TES units). FIRES may also be able to avoid a costly transformer in cases where the electric heater system is configured to use the line voltage without step-down. Regarding higher containment pressures, vessel cost scales linearly (Eq. (26)), such that a 10 bar pressure vessel of the same size increases the vessel cost by about 40%, a relatively modest increase with respect to other components and the economies of scale at work. This suggests FIRES is economically promising for coupling with high pressure NGCC and NACC power cycles as a round-trip electricity storage device in longer term deployment.

6.2. Market performance

Table 4 shows the simulated financial earnings of a FIRES unit in a market of high renewable penetration, northwestern Iowa. Results were calculated based on energy market data for the years 2013 and 2014. The price of electricity was negative approximately 5% of the time in each year, and the price was lower than the equivalent heating price of natural gas approximately 57% of the time across both years [43–45]. The ability to take advantage of this electricity as a heating source in place of natural gas would be economically favorable to ethanol plants and other industrial users of northwestern Iowa while also benefitting low-carbon generators and reducing emissions.

Table 4
Summary of FIRES market performance.

Western Iowa FIRES Market Performance (DQR = 0.1 h^{-1}, CQR = 0.2 h^{-1})		
Total stored energy value	$/kWh/yr	$16.67
Total stored energy cost	$/kWh/yr	$8.24
Operating income	$/kWh/yr	**$8.43**

The simulated financial results are for a characteristic FIRES unit with constant CQR of 0.2 h^{-1} and constant DQR of 0.1 h^{-1}. Using the market price data, the revenue earned was calculated assuming heat is demanded at all times, and that FIRES may switch instantaneously between four states:

- Buying electricity and heating the brickwork at full input power while discharging heat to the customer at full output power.
- Buying electricity and heating the brickwork at sufficient input power to exactly maintain the quantity of stored heat while discharging heat to the customer at full output power. (i.e. heat input equals heat output, no storage change)
- Discharging stored heat to the customer at full output power.
- Standing by inactive, because electricity is too expensive to buy and there is no stored heat available to discharge.

With the availability of day-ahead electricity market prices, FIRES units may be operated to maximize profit by preferentially charging at the lowest-bid prices of each day. Savings were calculated by subtracting the total cost of energy stored in FIRES from its equivalent natural gas value.

The profit earned by a FIRES unit in this market were found to be $8.43/kWh-yr. Compared to the estimated investment cost near $10/kWh, FIRES operated in this market would pay for itself within the second year, and provide returns on investment in subsequent years.

Where this discussion assumes that FIRES is a "price-taker" within the market, it is important to note that if many FIRES units were installed, the market would become saturated. The FIRES capacity installed in a market will depend on the relative availability of low-value electricity.

7. Conclusions

Findings of this work suggest that E-TES such as FIRES deserves greater focus in the ongoing discussions of grid-scale energy storage solutions. In the short term FIRES can electrify high temperature industries to take advantage of low-value electricity and mutually benefit the industry and low carbon generators. The low component cost for heat storage and the ever-rising efficiency of combined cycle technology make FIRES coupled with power cycles an attractive electricity storage alternative to batteries and geography-dependent mechanical storage technologies. Development of FIRES may open simultaneous pathways for decarbonization of both the industrial heating market and electricity grid.

Key questions regarding the charge, discharge and insulation capabilities of FIRES were addressed herein. Charge and discharge periods of only a few hours were found to be reasonably achievable – signifying comfortable daily cycling, and suggesting that FIRES may be operated in response to unexpected changes in low-carbon electricity production brought by intermittent clouds or other perturbations in electricity supply and demand. Concurrently, FIRES was found to retain heat with low leakage for over a week if necessary, making it also suitable for multi-day cycles. Simple damper and bypass actuation was shown to maintain the nominal discharge rate during cooldown for a large fraction of FIRES heat capacity, typically 70–90%, with generally acceptable fan power requirements and thermal shock characteristics. Because of the simplified correlations and numerical methods used to simulate heat transfer, results are approximate and should be taken as holistic indicators of FIRES's relative capabilities over the design space; the design and modeling of an application-specific FIRES unit should be done with more sophisticated tools, e.g. a commercial 3-dimensional finite element package.

Estimates of component cost and installation factors suggest that an overall cost of FIRES near $10/kWh is achievable following the maturation of the building process, which is based on commonplace

equipment and materials. In the context of a present-day energy market, specifically northwestern Iowa, FIRES would earn approximately $8.43/kWh per year, indicating an economic incentive for deployment. More work may be done regarding the FIRES's cost sensitivity to capacity. Not explored herein is the cost analysis of retrofitting industrial plants with FIRES.

The technology and components required for the base case FIRES unit are available today. Long term FIRES units require further research and development to be coupled with higher-temperature and high-pressure systems. Ongoing and future work on FIRES concerns the development of an inexpensive reliable conductive firebrick regenerator for a DRH charging system, and integration of FIRES within pressure boundaries of power cycles.

Acknowledgements

This work was supported through the INL National Universities Consortium (NUC) Program under DOE Idaho Operations Office Contract DE-AC07-05ID14517, and Exelon Corporation.

Author contributions

D.S. contributed the main part of research design, simulation and analysis. D.C. contributed the western Iowa market analysis. C.F. oversaw and guided the research and analysis. D.S. wrote the paper, and D.C. and C.F. edited the paper.

Competing interests

The authors declare no competing financial interests.

Appendix A. Supplementary material

Supplementary data to this article can be found online at https://doi.org/10.1016/j.apenergy.2019.03.100.

References

[1] Hirth L. The market value of variable renewables, the effect of solar wind power variability on their relative prices. Energy Econ 2013;38:218–36.
[2] Hirth L. The optimal share of variable renewables: how the variability of wind and solar power affects their welfare-optimal development. Energy J 2015;36(1).
[3] Massachusetts Institute of Technology Energy Initiative. The future of solar energy. Massachusetts Institute of Technology; 2015.
[4] Chen H, et al. Progress in electrical energy storage system: a critical review. Prog Nat Sci 2009;19(3):291–312.
[5] Fernandes, et al. Thermal energy storage: how previous findings determine current research priorities. Energy 2012;39(1):246–57.
[6] U.S. Department of Energy. Grid energy storage. December 2013. Retrieved 31 July 2017 from http://energy.gov/sites/prod/files/2014/09/f18/Grid%20Energy%20Storage%20December%202013.pdf.
[7] Schmidt, et al. "The future cost of electrical energy storage based on experience rates". Nat Energy 2017;2(1). https://doi.org/10.1038/nenergy.2017.110.
[8] Sardeshpande V, et al. Performance analysis for glass furnace regenerator. Appl Energy 2011;88(12).
[9] Laing D, Zunft S. Using concrete and other solid storage media in thermal energy storage (TES) systems. In: Cabeza LF, editor. Advances in thermal energy storage systems, Ch. 4. Elsevier; 2015. p. 65–86.
[10] Gasia J, et al. Review on system and materials requirements for high temperature thermal energy storage. Part 1: General requirements. Renew Sustain Energy Rev 2017;75:1320–38.
[11] Gil, et al. State of the art on high temperature thermal energy storage for power generation. Part 1—Concepts, materials and modellization. Renew Sustain Energy Rev 2010;14(1):31–55.
[12] China Household Electrical Appliances Association. China's coal-to-electricity policy to further boost market growth, setting central heating a new trend. May 2018. Retrieved 18 September 2018 from http://en.cheaa.org/contents/476/7689.html.
[13] Stack D. Conceptual design and performance characteristics of firebrick resistance-heated energy storage for industrial heat supply and variable electricity production. MS thesis. Department of Nuclear Science and Engineering, Massachusetts Institute of Technology; 2017.
[14] Forsberg C, et al. Converting excess low-price electricity into high-temperature stored heat for industry and high-value electricity production. Electr J 2017;30(6):42–52.
[15] Lawrence Livermore National Laboratory. Estimated U.S. energy consumption in 2016: 93.7 quads. Retrieved 27 September 2017 from https://flowcharts.llnl.gov/content/assets/images/energy/us/Energy_US_2016.png.
[16] Andreades C, et al. Reheat-air brayton combined cycle power conversion design and performance under nominal ambient conditions. J Eng Gas Turbines Power 2014;136.
[17] SIEMENS GAMESA. Same forces. New rules. introducing electric thermal energy storage (ETES). Retrieved 9 February 2019 from https://www.siemensgamesa.com/-/media/siemensgamesa/downloads/en/products-and-services/hybrid-power-and-storage/etes/siemens-gamesa-storage-etes-storage-brochure-en.pdf.
[18] Zunft S et al. Electricity storage with adiabatic compressed air energy storage: results of the BMWi-project ADELE-ING. International ETG congress 2017, Bonn, Germany; 2017. p. 1–5.
[19] Zunft S et al. Adiabate Druckluftspeicher für die Elektrizitätsversorgung – der ADELE-Wärmespeicher. Kraftwerkstechnik, vol. 4. Dresden: TK Verlag. p. 749–57.
[20] Daniele Corus. Daniele corus hot blast stoves: once in a lifetime. Retrieved 18 September 2018 from http://www.danieli-corus.com/media/Stoves.pdf.
[21] Willmott AJ. Regenerative heat exchangers. Thermopedia 2011. https://doi.org/10.1615/AtoZ.r.regenerative_heat_exchangers.
[22] Min JK, et al. High temperature heat exchanger studies for applications to gas turbines. Heat Mass Transf 2009;46:175–86.
[23] Springer Handbook of Condensed Matter and Materials Data. W. Martienssen and H Warlimont. Germany; 2005.
[24] Powell RW et al. Thermal conductivity of selected materials. NSRDS-NBS 8, 1966. Retrieved 18 September 2018 from https://srd.nist.gov/NSRDS/NSRDS-NBS-8.pdf.
[25] National Institute of Standards and Technology. Sintered silicon carbide (SiC). Retrieved 18 September 2018 from http://srdata.nist.gov/CeramicDataPortal/Pds/Scdscs.
[26] Kanthal®. Resistance heating alloys and systems for industrial furnaces. Retrieved 18 September 2018 from https://www.kanthal.com/globalassets/kanthal-global/downloads/materials-in-wire-and-strip-form/resistance-heating-wire-and-strip/home-appliance_s-ka026-b-eng_lr.pdf.
[27] Kanthal®. Kanthal® Globar® SD silicon carbide heating elements. Retrieved on 18 September 2018 from https://www.kanthal.com/globalassets/kanthal-global/downloads/furnace-products-and-heating-systems/heating-elements/sic-heating-elements/s-ka011-b-eng-2011-06.pdf.
[28] Kanthal®. Kanthal super electric heating elements: products and accessories. Retrieved 18 September 2018 from https://www.kanthal.com/globalassets/kanthal-global/downloads/furnace-products-and-heating-systems/heating-elements/mosi2-heating-elements/s-ka058-b-eng-2012-01.pdf.
[29] Department of Energy. Quadrennial technology review: an assessment of energy technologies and research opportunities; September 2015. p. 188.
[30] Deshmukh Y. Electric resistance heating. Industrial heating: principles, techniques, materials, application and design, Ch. 9. Taylor & Francis; 2005.
[31] Stack D, Forsberg C. Using conductive firebrick resistance heating to enable very high-temperature heat storage in nuclear gas turbine systems. Transactions of the American Nuclear Society, vol. 116, San Francisco, California; June 11–15, 2017. 2017.
[32] Hutchinson I. A student's guide to numerical methods. Cambridge University Press; 2015.
[33] Gnielinski. Neue Gleichungen für den Wärme- und den Stoffübergang in turbulent durchströmten Rohren und Kanälen" (Translation: New equations for heat and mass transfer in turbulent pipes and ducts) 1975;vol. 41, no. 1:8–16.
[34] Norris RH. Some simple approximate heat transfer correlations for turbulent flow in ducts with rough surfaces. In: Bergles AE, Webb RL, editors. Augmentation of convective heat transfer. New York: ASME; 1970.
[35] Cengel Y, Ghajar A. Heat and mass transfer: fundamentals and application. fourth ed. McGraw-Hill; 2011.
[36] Mills AF, Coimbra CFM. Heat transfer: third edition. Temporal Publishing; 2016.
[37] Todreas N, Kazimi M. Nuclear systems I: thermal hydraulic fundamentals. Taylor & Francis; 1993.
[38] Lu TJ, Fleck NA. The thermal shock resistance of solids. Acta Mater 1998;46(13):4755–68.
[39] Zunft S, et al. A design study for regenerator-type heat storage in solar tower plants-results and conclusions of the HOTSPOT project. Energy Procedia 2014;49:1088–96.
[40] Brown T. Engineering economics and economic design for process engineers. Taylor & Francis; 2006.
[41] Garrett DE. Chemical engineering economics. Van Nostrand Reinhold; 1989.
[42] Office of Electricity Delivery and Energy Reliability. Large power transformers and the U.S. Electricity Grid. Department of Energy. June 2012. Retrieved 1 August 2018 from https://www.energy.gov/oe/downloads/large-power-transformers-and-us-electric-grid-report-june-2012.
[43] MISO Energy. LMP contour map. Retrieved 18 September 2018 from https://api.misoenergy.org/MISORTWD/lmpcontourmap.html.
[44] MISO Energy. Market reports. Retrieved 18 September 2018 from https://www.misoenergy.org/markets-and-operations/market-reports/#t=10&p=0&s=MarketReportPublished&sd=desc.
[45] US EIA. Natural gas. Retrieved 18 September 2018 from http://www.eia.gov/dnav/ng/ng_pri_sum_dcu_sia_m.htm.
[46] Morgan Thermal Ceramics. Insulating Firebricks JM. Retrieved 18 September 2018 from http://www.lynnmfg.com/wp-content/uploads/2015/10/DATA-TC-1-11-10E.pdf.